Science Advances
AAAS

advances.sciencemag.org/cgi/content/full/7/19/eabd5684/DC1

Supplementary Materials for

Optogenetic pacing of medial septum parvalbumin-positive cells disrupts temporal but not spatial firing in grid cells

Mikkel Elle Lepperød, Ane Charlotte Christensen, Kristian Kinden Lensjø, Alessio Paolo Buccino, Jai Yu, Marianne Fyhn, Torkel Hafting*

*Corresponding author. Email: torkel.hafting@medisin.uio.no

Published 5 May 2021, *Sci. Adv.* **7**, eabd5684 (2021)
DOI: 10.1126/sciadv.abd5684

This PDF file includes:

Supplementary information

The supplementary information contains figures S1-11, tables S1-6 and a supplementary discussion related to the analysis in Figure 3.

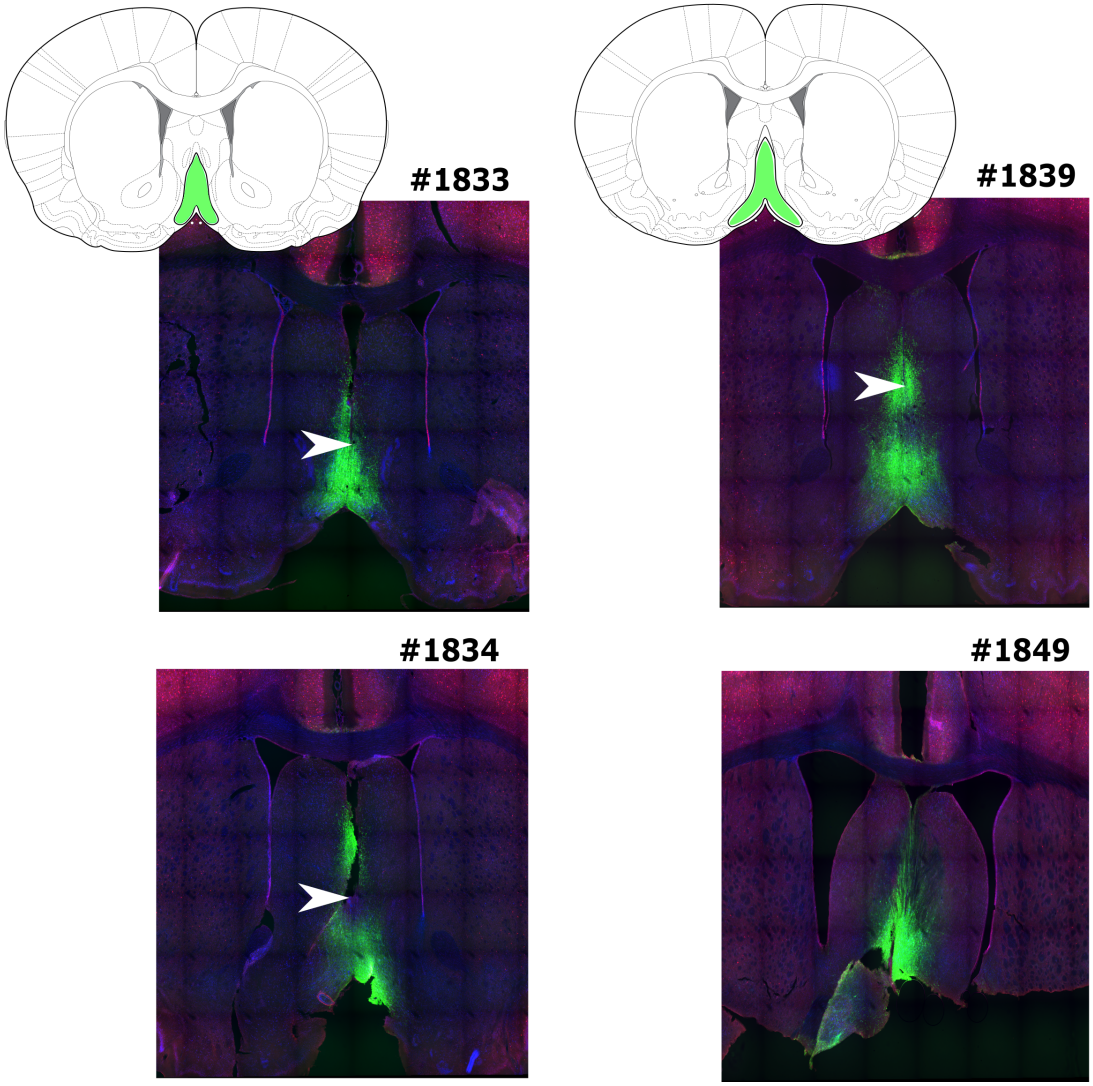

Figure S1: **Virus expression and optic fiber location in the medial septal area (MSA)**. Outline of coronal sections from all 4 animals showing ChR2 expression in MSA. Rat number is denoted above each picture. Illustrations of an entire coronal section highlights the MSA at two different anterior-posterior positions in green. The deepest position of the optic fiber that could be identified is marked with a white arrow. Note that the optic fiber trace could not be located in sections from rat # 1849, hence the missing arrow.

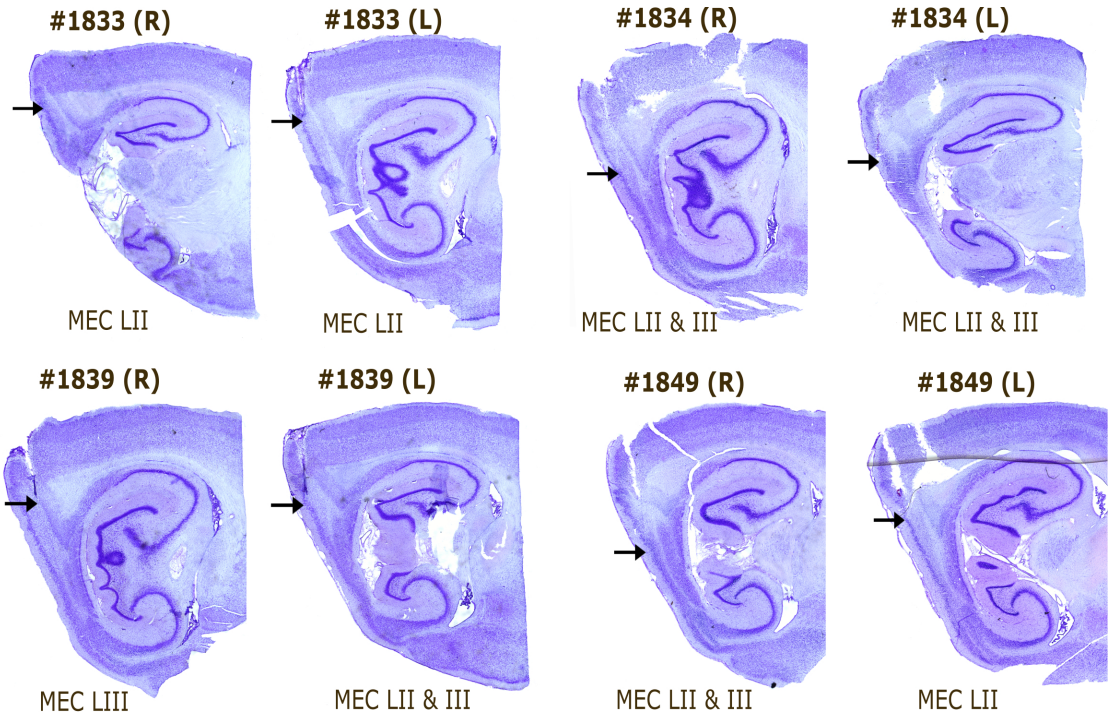

Figure S2: **Tetrode tracks in medial entorhinal cortex.** Sagittal sections from all 4 rats used in this study, stained for cell bodies to identify the position of tetrodes. Rat number and hemisphere is denoted above each section and recording positions in MEC are written below. The deepest located recording position is marked with a black arrow.

entity	Gridcell	BS not gridcell	NSi	NSni
1833	94	165	16	52
1834	14	216	4	7
1839	19	70	11	5
1849	8	229	8	23

Table S1: **Cell count from each animal**

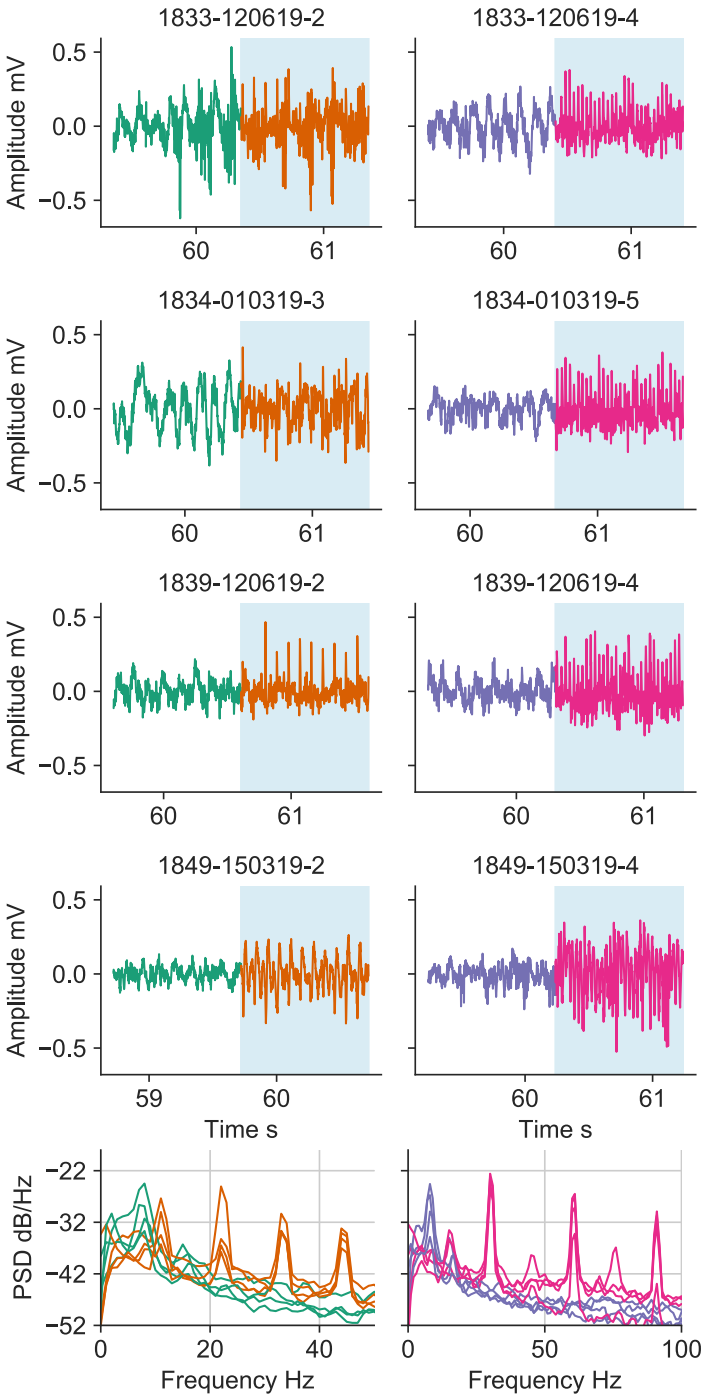

Figure S3: **Examples of raw traces** Each row of raw LFP traces 1 sec before and after stimulation onset. PSD of 60 sec before and after is shown in the bottom panel.

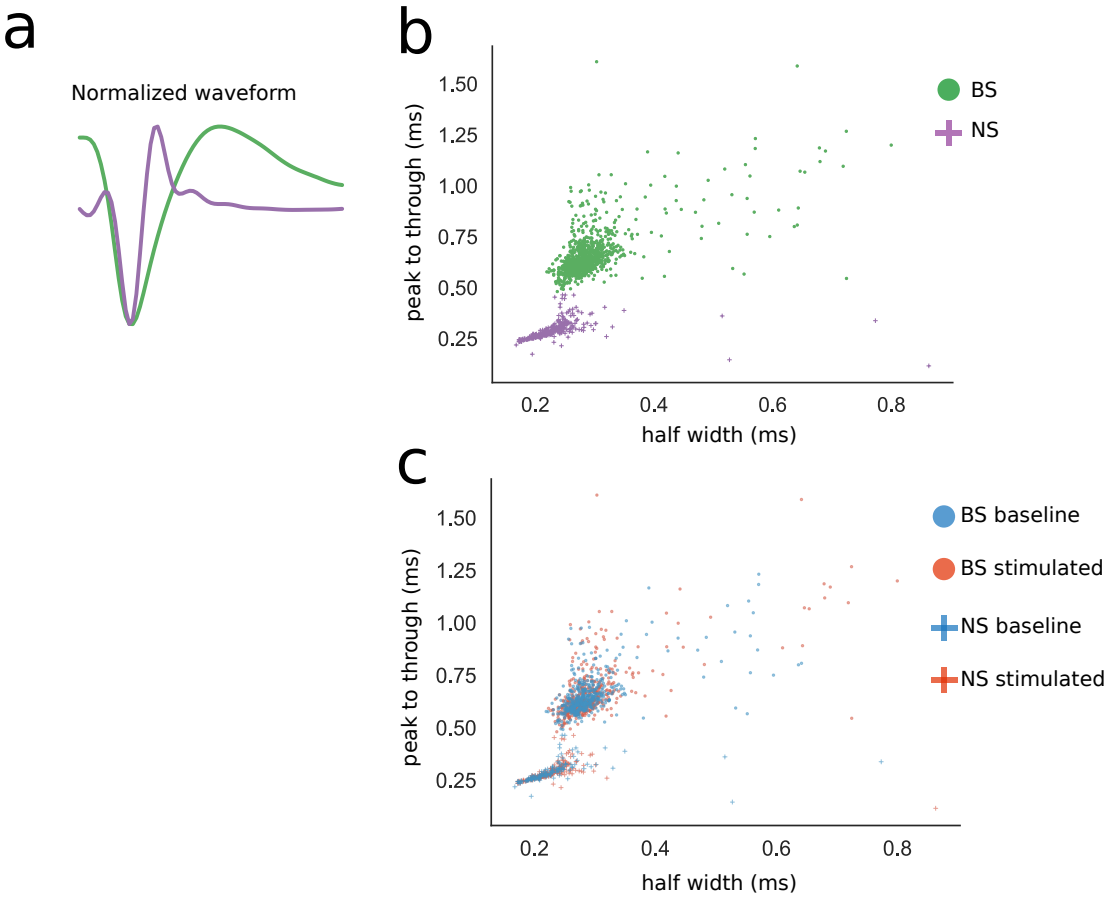

Figure S4: **Separation of broad and narrow spiking units. a**) Normalized waveforms for one broad spiking (BS) putative excitatory neurons (green), and one narrow spiking (NS) putative inhibitory neuron (purple). **b**) Separation of broad and narrow spiking units by plotting peak to trough time against the width or half amplitude using kmeans. Green circles represent units categorized as broad spiking and purple cross represent units categorized as narrow spiking. **c**) Similar plot as **b** divided into baseline and stimulation sessions. Optogenetic stimulation in MSA did not alter the parameters used to separate units into broad and narrow spiking.

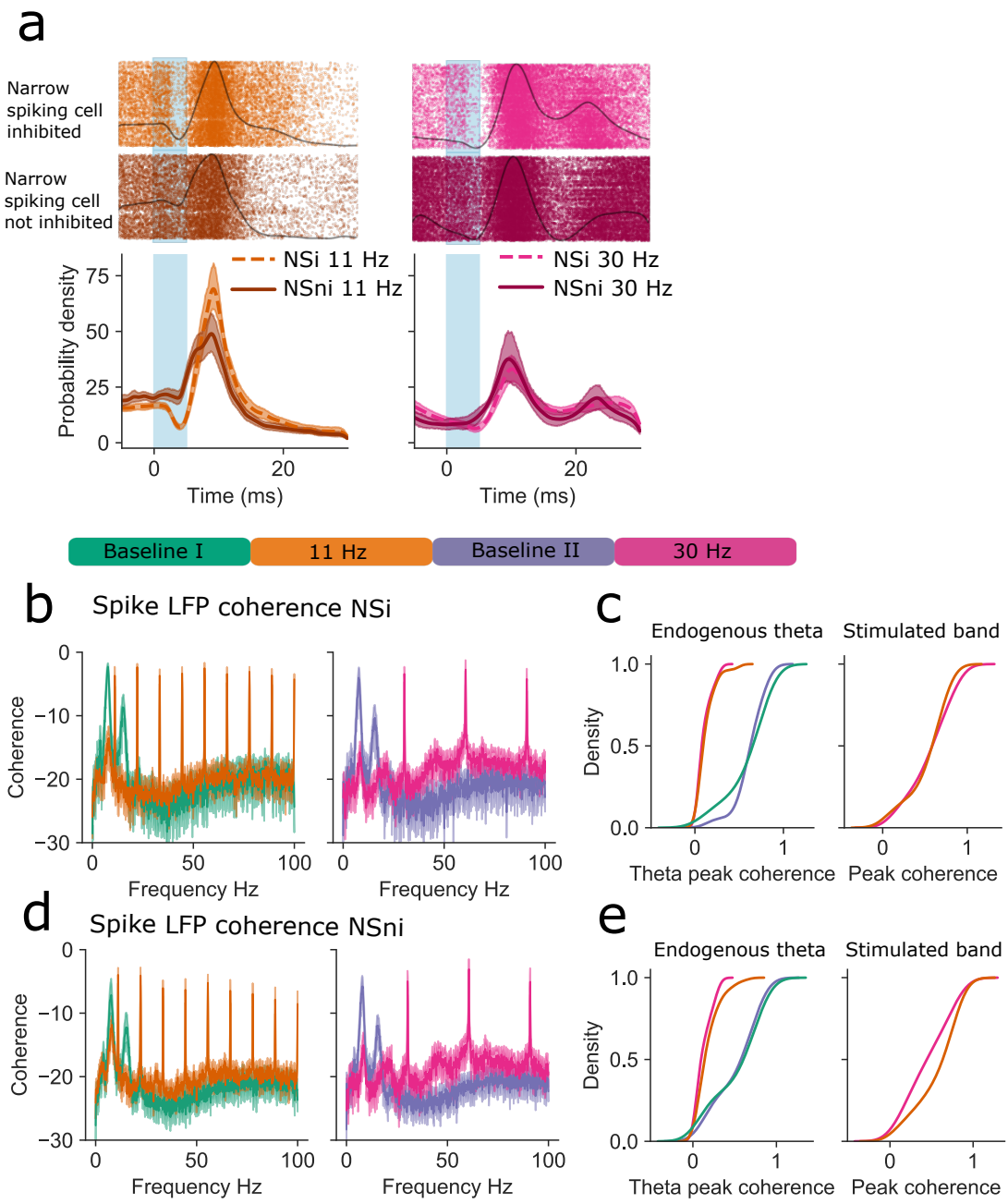

Figure S5: **Narrow spiking units show different responses to MSA stimulation**. **a**) Raster plot of single unit spiking responses from one narrow spiking cells that was inhibited by the stimulus (NSi) (top) and one narrow spiking unit that was not inhibited (NSni) (bottom). Probability density for the whole population of NSi and NSni cells show that NSi cells are strongly inhibited approximately 3-5 ms after stimulus onset. **b**) Spike LFP coherence for NSi cells show a strong coherency with endogenous theta for both Baseline sessions (Baseline I & II). This was significantly reduced during both 11 Hz and 30 Hz stimulations. **c**) Density plots show that endogenous theta was strongly reduced during stimulation, while peak coherency was similar for both frequencies. **d**) Similar to **b** for NSni cells. **e**) Similar to **c** for NSni cells.

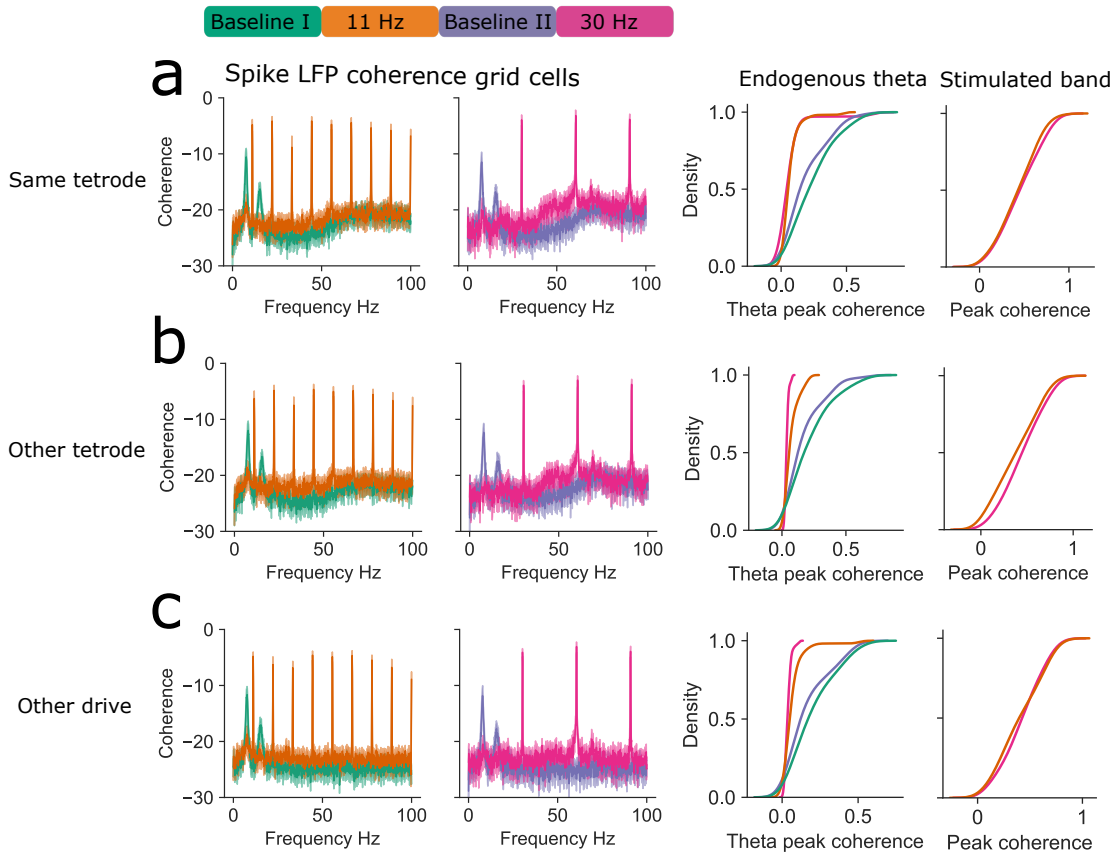

Figure S6: **Spike LFP coherence using LFP recorded from a different tetrode or hemisphere show that high spike LFP coherence is not a result of action potentials from the recorded grid cells a**) Spike LFP coherence for grid cells using LFP from the same tetrode show a strong coherency with endogenous theta. This coherence was significantly reduced during both 11 Hz and 30 Hz stimulations. Density plots show that endogenous theta was strongly reduced during stimulation, while peak coherency was similar for both stimulation frequencies.**b**) Spike LFP coherence for grid cells using LFP from a different tetrode. **c**) Spike LFP coherence for grid cells using LFP simultaneously recorded from the opposite hemisphere. Grid cells show similar coherency with endogenous theta and with the stimulated frequency as in **a** and **b**.

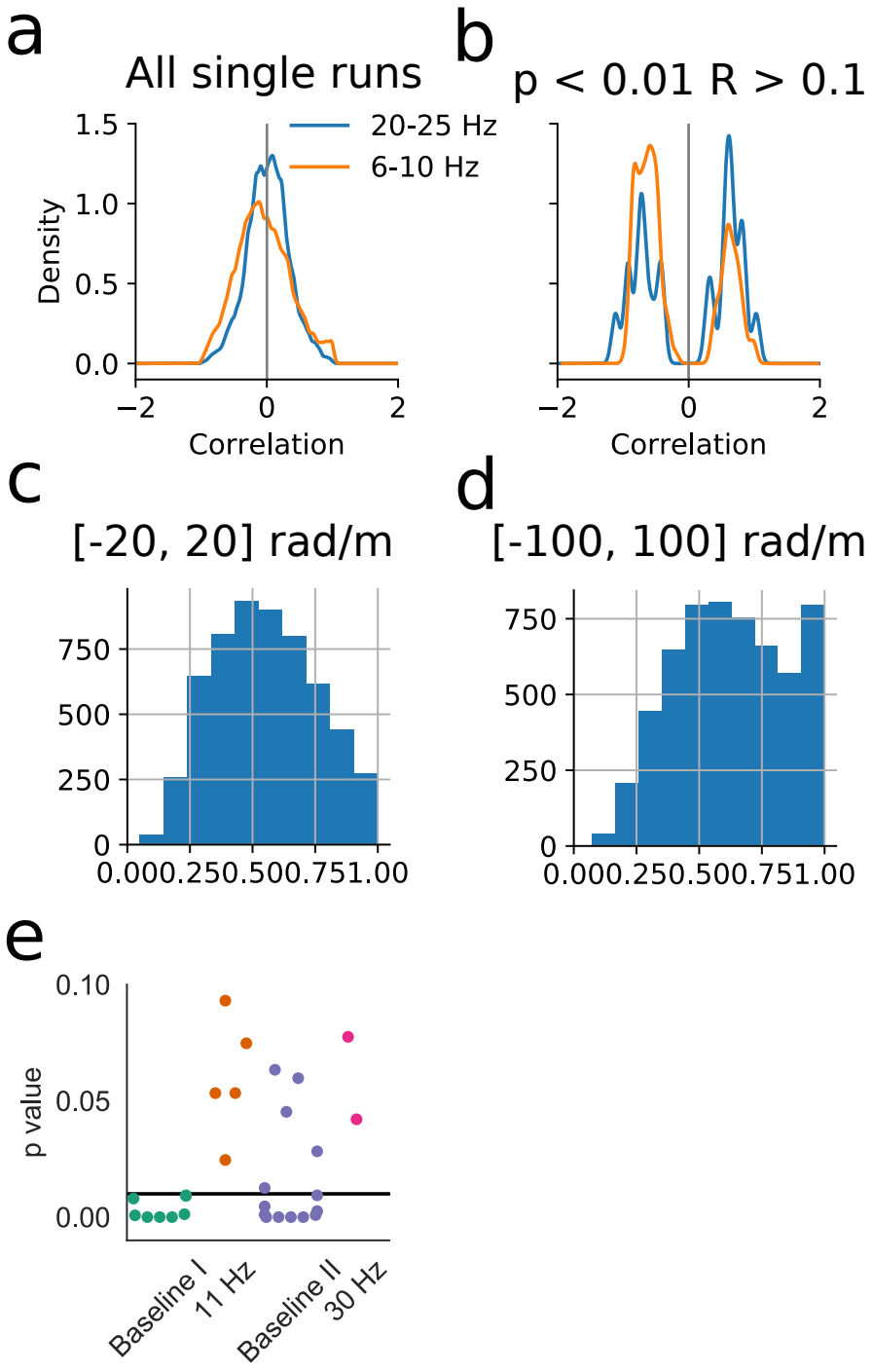

Figure S7: **Invalidating usage of single runs to assess loss of phase precession a)** Distribution of circular-linear correlation values for runs in the square arena. 6-10(20-25) Hz denotes the band pass filter limit of theta and "random" band of the LFP. **b)** Distribution of circular-linear correlation values for runs in the square arena in which only significant phase precession is kept ($p < 0.01$ and $R > 0.1$). **c** Distribution of goodness of fit (R) with slope limit at [-20, 20] rad/m. **d** Distribution of goodness of fit (R) with slope limit at [-100, 100] rad/m, note the shift towards $R = 1$. **e** p values for the same analysis as in Fig. 3 but with in-field detection performed on the firing rate with threshold = mean + standard deviation of the full firing rate. Only points with p value below 0.10 is shown in the figure.

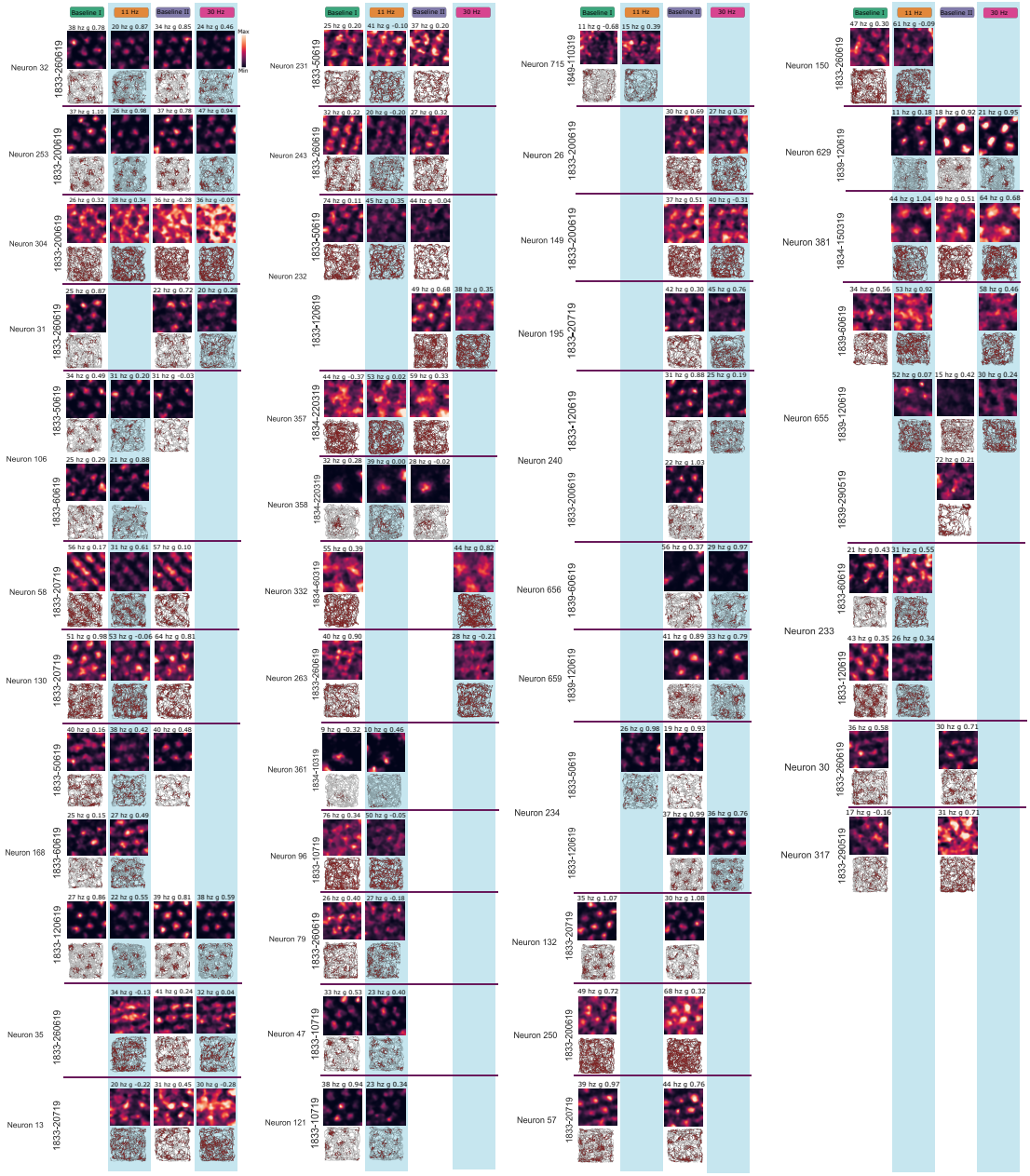

Figure S8: **Overview of all grid cells recorded during baseline and stimulation sessions** Rate maps (top) and running path with spikes superimposed (bottom) are indicated for each unit. Max rate and gridness is shown above each rate map. Note that the color coding of the ratemaps are relative to the first recording session for each unit, thus brighter colors in following sessions indicate higher firing rates while darker colors indicate reduced firing rates. Unit name, rat ID and recording date is indicated to the left of the rate maps. Experimental paradigm is shown above each column and optogenetic stimulation sessions is marked in blue shading. Note that some units are recorded over several days and individual units are therefore separated by a purple line.

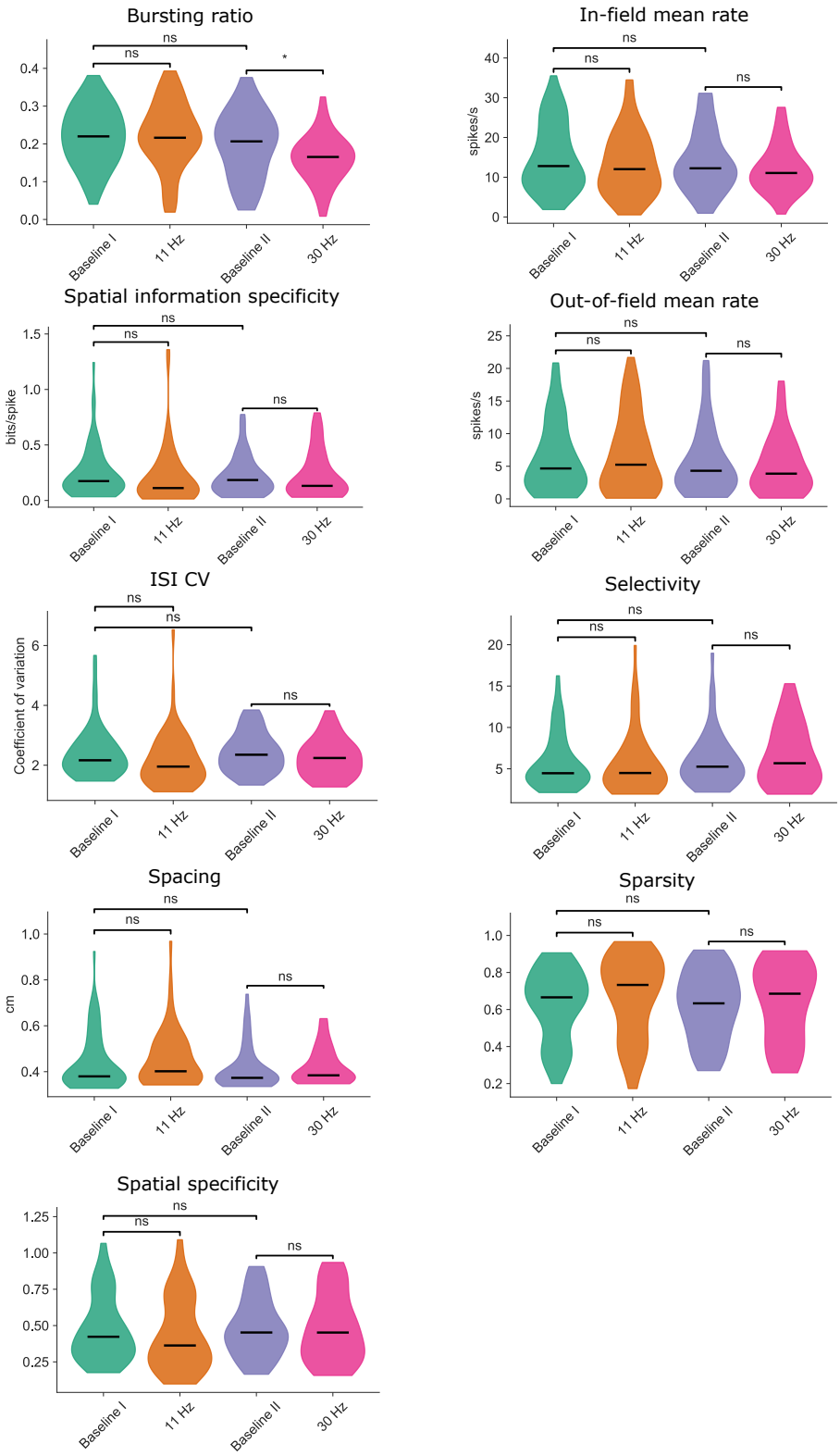

Figure S9: **Overview of grid cell statistics** Violin plots show the effect in temporal and spatial properties of grid cells during optostimulation. ns = non significant, $p^* < 0.05$, linear mixed model.

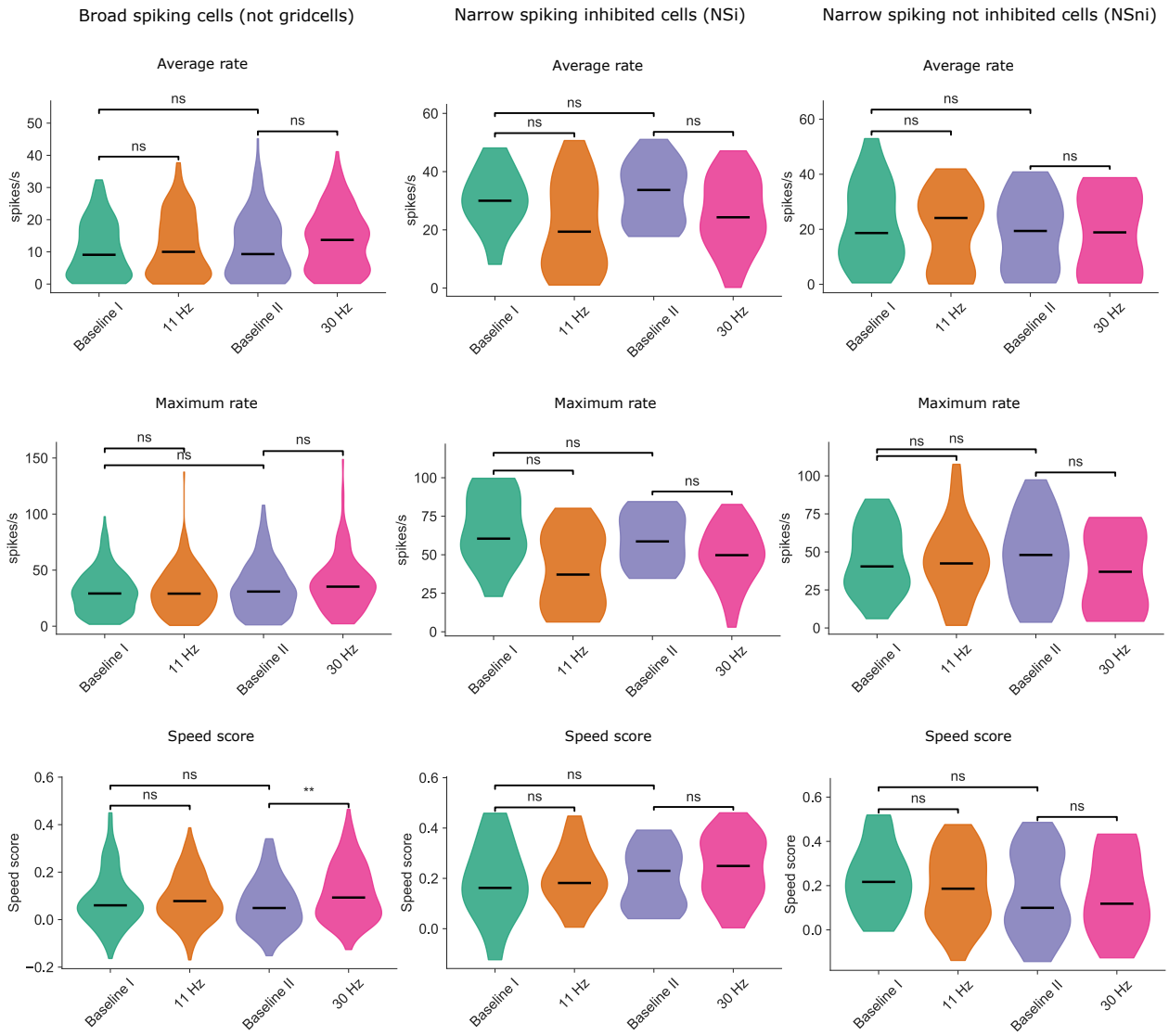

Figure S10: **Effect of optostimulation on other cell types**. Violin plots showing change in average rate, maximum rate and speed score between baseline and stimulation sessions. This is shown for broad spiking (non-grid cells), narrow spiking inhibited (NSi) and narrow spiking not inhibited (NSni) cells separately. ns = non significant, $^{**}p < 0.01$, linear mixed model.

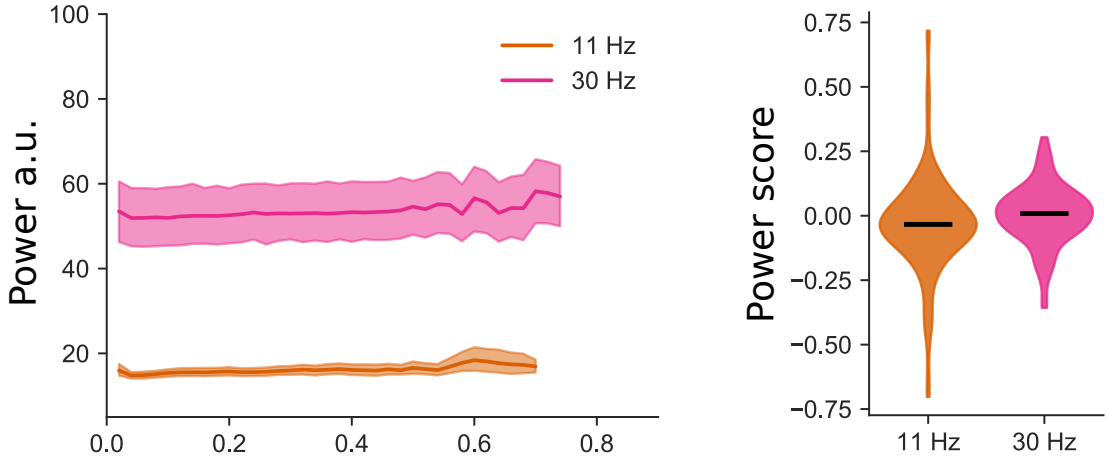

Figure S11: **LFP power not speed modulated in the stimulation frequency band** Left: power vs running speed. Right: Pearson correlation coefficient of speed vs power.

Weighted mean ± s.e.m.	Baseline I	11 Hz
Average rate	9.83 ± 0.935 (63)	11 ± 1.03 (56)
Gridness	0.369 ± 0.0556 (63)	0.403 ± 0.051 (56)
Sparsity	0.662 ± 0.0241 (63)	0.713 ± 0.0306 (56)
Selectivity	5.28 ± 0.428 (63)	5.42 ± 0.591 (56)
Information rate	1.36 ± 0.0858 (63)	0.929 ± 0.0687 (56)
Information specificity	0.255 ± 0.0344 (63)	0.221 ± 0.0449 (56)
Max rate	35.8 ± 2.05 (63)	35.8 ± 2.21 (56)
Interspike interval cv	2.19 ± 0.0889 (63)	2.01 ± 0.145 (56)
Burst event ratio	0.227 ± 0.0111 (63)	0.231 ± 0.0115 (56)
In-field mean rate	15.3 ± 1.19 (63)	15.8 ± 1.29 (56)
Out-field mean rate	7.34 ± 0.79 (63)	8.76 ± 0.901 (56)
Max-field mean rate	12.1 ± 1.27 (35)	10.9 ± 1.62 (31)
Specificity	0.417 ± 0.0288 (63)	0.386 ± 0.0353 (56)
Speed score	0.106 ± 0.0108 (63)	0.0945 ± 0.0119 (56)
Spacing	0.559 ± 0.0199 (63)	0.537 ± 0.0198 (56)
Field area	0.446 ± 0.00757 (63)	0.433 ± 0.00782 (56)
Head mean vec len	0.0875 ± 0.00854 (63)	0.0771 ± 0.00861 (56)
Border score	0.207 ± 0.013 (63)	0.206 ± 0.0119 (56)
Weighted mean ± s.e.m.	Baseline II	30 Hz
Average rate	10.4 ± 1 (46)	8.5 ± 1.12 (35)
Gridness	0.527 ± 0.0371 (46)	0.573 ± 0.0487 (35)
Sparsity	0.656 ± 0.032 (46)	0.638 ± 0.0366 (35)
Selectivity	6.24 ± 0.672 (46)	6.75 ± 0.675 (35)
Information rate	1.27 ± 0.104 (46)	1.14 ± 0.112 (35)
Information specificity	0.232 ± 0.0343 (46)	0.243 ± 0.0375 (35)
Max rate	42.2 ± 2.43 (46)	37 ± 2.53 (35)
Interspike interval cv	2.16 ± 0.0803 (46)	2.27 ± 0.107 (35)
Burst event ratio	0.234 ± 0.0114 (46)	0.177 ± 0.0118 (35)
In-field mean rate	16.8 ± 1.23 (46)	13.1 ± 1.26 (35)
Out-field mean rate	7.76 ± 0.857 (46)	5.97 ± 0.875 (35)
Max-field mean rate	16.9 ± 2.55 (33)	7.77 ± 1.2 (19)
Specificity	0.434 ± 0.0309 (46)	0.467 ± 0.0398 (35)
Speed score	0.0874 ± 0.00801 (46)	0.0738 ± 0.0099 (35)
Spacing	0.525 ± 0.0159 (46)	0.492 ± 0.0147 (35)
Field area	0.438 ± 0.00863 (46)	0.442 ± 0.00927 (35)
Head mean vec len	0.0666 ± 0.00712 (46)	0.0878 ± 0.00791 (35)
Border score	0.181 ± 0.013 (46)	0.192 ± 0.015 (35)

Table S2: **Statistics for grid cell firing properties 1** Shows weighted mean ± standard error of the mean and number of units (n).

LMM	Baseline I - 11 Hz	Baseline II - 30 Hz
Average rate	β=0.594, p=0.695	β=-0.621, p=0.813*
Gridness	β=0.0265, p=0.851	β=0.0271, p=0.861
Sparsity	β=0.0256, p=0.253	β=0.0194, p=0.583
Selectivity	β=-0.196, p=0.885*	β=-0.0414, p=0.933
Information rate	β=-0.395, p=0.0158	β=-0.0267, p=0.949
Information specificity	β=-0.0372, p=0.757*	β=-0.0205, p=0.33
Max rate	β=-1.21, p=0.764	β=-1.61, p=0.744
Interspike interval cv	β=-0.158, p=0.052	β=-0.0144, p=0.957
Burst event ratio	β=0.00504, p=0.774	β=-0.0386, p=0.0128
In-field mean rate	β=0.052, p=0.981	β=-0.454, p=0.558
Out-field mean rate	β=0.701, p=0.506	β=-0.0875, p=0.912
Max-field mean rate	β=-4.22, p=0.245	β=0.181, p=0.983
Specificity	β=-0.0258, p=0.19	β=0.0152, p=0.761
Speed score	β=-0.0129, p=0.529	β=-0.0125, p=0.382**
Spacing	β=-0.0327, p=0.29	β=-0.0263, p=0.194
Field area	β=-0.0147, p=0.236	β=-0.00119, p=0.897
Head mean vec len	β=-0.00484, p=0.807	β=0.0112, p=0.578
Border score	β=0.00181, p=0.963	β=0.0366, p=0.558
LMM	Baseline I - Baseline II	11 Hz - 30 Hz
Average rate	β=0.306, p=0.822	β=-1.18, p=0.608
Gridness	β=0.0326, p=0.588**	β=0.116, p=0.319
Sparsity	β=-0.00342, p=0.951	β=-0.0397, p=0.66*
Selectivity	β=1.03, p=0.576	β=1.07, p=0.163
Information rate	β=-0.1, p=3.43e-05	β=0.25, p=0.158
Information specificity	β=-0.0299, p=0.236	β=0.056, p=0.216
Max rate	β=3.45, p=0.33	β=6.49, p=0.0942
Interspike interval cv	β=-0.012, p=0.935**	β=0.408, p=0.0945
Burst event ratio	β=-0.0103, p=0.75	β=-0.0562, p=0.212*
In-field mean rate	β=0.568, p=0.71	β=-1.01, p=0.687
Out-field mean rate	β=0.363, p=0.693	β=-1.87, p=0.306
Max-field mean rate	β=4.11, p=0.728	β=-0.69, p=0.901*
Specificity	β=-0.0102, p=0.933	β=0.0448, p=0.419
Speed score	β=0.00945, p=0.68	β=0.0165, p=0.843
Spacing	β=-0.0291, p=0.439	β=-0.0378, p=0.141
Field area	β=-0.0071, p=0.666	β=-0.00257, p=0.863
Head mean vec len	β=-0.0139, p=0.197**	β=0.00226, p=0.875
Border score	β=-0.0283, p=0.5	β=-0.00217, p=0.952

Table S3: **Statistics for grid cell firing properties 2** Show results from a linear mixed model, β and p denotes effect size and p value respectively. In these cases we altered the model, alterations are marked by adding a * or ** to the pvalues (see methods section under Quantification and statistical analysis for a description of the different alterations)

Weighted mean ± s.e.m.	Baseline I	11 Hz
Average rate	29.8 ± 2.69 (12)	19.4 ± 3 (25)
Max rate	67.2 ± 6.1 (12)	37.3 ± 4.78 (25)
Interspike interval cv	1.94 ± 0.406 (12)	1.45 ± 0.0796 (25)
Burst event ratio	0.256 ± 0.021 (12)	0.198 ± 0.0218 (25)
Speed score	0.15 ± 0.0399 (12)	0.18 ± 0.0203 (25)
Head mean vec len	0.048 ± 0.00698 (12)	0.0434 ± 0.00536 (25)
Border score	0.251 ± 0.018 (12)	0.274 ± 0.0162 (25)
Weighted mean ± s.e.m.	Baseline II	30 Hz
Average rate	26.6 ± 2.26 (17)	22.8 ± 2.15 (32)
Max rate	48.8 ± 4.2 (17)	43.7 ± 3.27 (32)
Interspike interval cv	1.75 ± 0.101 (17)	1.59 ± 0.151 (32)
Burst event ratio	0.282 ± 0.0173 (17)	0.197 ± 0.0146 (32)
Speed score	0.172 ± 0.025 (17)	0.205 ± 0.0192 (32)
Head mean vec len	0.0398 ± 0.00297 (17)	0.0589 ± 0.00667 (32)
Border score	0.247 ± 0.0189 (17)	0.241 ± 0.013 (32)
LMM	Baseline I - 11 Hz	Baseline II - 30 Hz
Average rate	β=-7.4, p=0.125**	β=-0.995, p=0.801
Max rate	β=-29.2, p=3.72e-05*	β=-7.52, p=0.092**
Interspike interval cv	β=-0.815, p=0.0569	β=-0.213, p=0.000106
Burst event ratio	β=-0.00152, p=0.977	β=-0.0832, p=1.11e-38*
Speed score	β=0.0181, p=0.686	β=0.0346, p=0.296
Head mean vec len	β=-0.0107, p=0.549	β=0.0192, p=0.241*
Border score	β=0.043, p=0.26	β=-0.00486, p=0.91
LMM	Baseline I - Baseline II	11 Hz - 30 Hz
Average rate	β=1.17, p=0.813	β=1.36, p=0.647
Max rate	β=-6.72, p=0.466	β=3.66, p=0.483
Interspike interval cv	β=-0.657, p=0.314	β=0.161, p=0.672
Burst event ratio	β=0.0423, p=7.79e-40	β=-0.0221, p=0.466
Speed score	β=-0.0167, p=0.539	β=0.0318, p=0.248
Head mean vec len	β=-0.0109, p=0.237	β=0.0137, p=0.267
Border score	β=0.0128, p=0.643	β=-0.0234, p=0.443

Table S4: **Statistics for NSi firing properties** Shows weighted mean ± standard error of the mean and number of units (n) and results from a linear mixed model, β and p denotes effect size and p value respectively. In these cases we altered the model, alterations are marked by adding a * or ** to the pvalues (see methods section under Quantification and statistical analysis for a description of the different alterations)

Weighted mean ± s.e.m.	Baseline I	11 Hz
Average rate	25.9 ± 3.34 (30)	21.8 ± 1.83 (32)
Max rate	48.8 ± 4.39 (30)	46.8 ± 3.76 (32)
Interspike interval cv	1.77 ± 0.229 (30)	1.57 ± 0.0939 (32)
Burst event ratio	0.251 ± 0.0145 (30)	0.238 ± 0.0172 (32)
Speed score	0.201 ± 0.0222 (30)	0.154 ± 0.0228 (32)
Head mean vec len	0.0729 ± 0.0176 (30)	0.0749 ± 0.0213 (32)
Border score	0.248 ± 0.0111 (30)	0.247 ± 0.0126 (32)
Weighted mean ± s.e.m.	Baseline II	30 Hz
Average rate	19.9 ± 2.4 (23)	20 ± 4.8 (12)
Max rate	51 ± 5.36 (23)	39.3 ± 8.57 (12)
Interspike interval cv	1.7 ± 0.162 (23)	1.72 ± 0.229 (12)
Burst event ratio	0.215 ± 0.0198 (23)	0.201 ± 0.0346 (12)
Speed score	0.12 ± 0.0336 (23)	0.13 ± 0.0347 (12)
Head mean vec len	0.0783 ± 0.0239 (23)	0.0981 ± 0.0415 (12)
Border score	0.236 ± 0.0155 (23)	0.238 ± 0.0256 (12)
LMM	Baseline I - 11 Hz	Baseline II - 30 Hz
Average rate	β=-1.57, p=0.656*	β=-0.994, p=0.838**
Max rate	β=-0.0671, p=0.989*	β=-4.69, p=0.754
Interspike interval cv	β=-0.0718, p=0.92	β=-0.104, p=0.681
Burst event ratio	β=0.000447, p=0.986*	β=-0.0288, p=0.693
Speed score	β=-0.0756, p=0.29	β=0.0133, p=0.887
Head mean vec len	β=0.00218, p=0.981	β=-0.00656, p=0.891
Border score	β=0.00486, p=0.909	β=-0.0264, p=0.687
LMM	Baseline I - Baseline II	11 Hz - 30 Hz
Average rate	β=-2.43, p=0.535*	β=2.63, p=0.691
Max rate	β=1.6, p=0.694	β=3.47, p=0.795
Interspike interval cv	β=-0.143, p=0.794	β=-0.242, p=0.362
Burst event ratio	β=-0.00723, p=0.935	β=-0.0664, p=0.218
Speed score	β=-0.0743, p=0.313	β=0.0132, p=0.898
Head mean vec len	β=-0.00407, p=0.939*	β=0.00769, p=0.784
Border score	β=-0.00313, p=0.925	β=-0.0138, p=0.786

Table S5: **Statistics for NSni firing properties** Shows weighted mean ± standard error of the mean and number of units (n) and results from a linear mixed model, β and p denotes effect size and p value respectively. In these cases we altered the model, alterations are marked by adding a * or ** to the pvalues (see methods section under Quantification and statistical analysis for a description of the different alterations)

Weighted mean ± s.e.m.	Baseline I	11 Hz
Average rate	10.1 ± 0.578 (211)	11.2 ± 0.631 (228)
Max rate	31 ± 1.32 (211)	30.4 ± 1.38 (228)
Interspike interval cv	2.47 ± 0.117 (211)	1.88 ± 0.0606 (228)
Burst event ratio	0.218 ± 0.00601 (211)	0.208 ± 0.00791 (228)
Speed score	0.105 ± 0.00912 (211)	0.0925 ± 0.00723 (228)
Head mean vec len	0.0998 ± 0.0065 (211)	0.0801 ± 0.00526 (228)
Border score	0.235 ± 0.00669 (211)	0.227 ± 0.00669 (228)
Weighted mean ± s.e.m.	Baseline II	30 Hz
Average rate	10.2 ± 0.73 (155)	12.4 ± 0.731 (161)
Max rate	30.3 ± 1.75 (155)	35.3 ± 1.87 (161)
Interspike interval cv	2.26 ± 0.151 (155)	1.82 ± 0.0593 (161)
Burst event ratio	0.203 ± 0.00841 (155)	0.184 ± 0.00743 (161)
Speed score	0.0807 ± 0.00863 (155)	0.119 ± 0.00968 (161)
Head mean vec len	0.0867 ± 0.00802 (155)	0.083 ± 0.00753 (161)
Border score	0.232 ± 0.00607 (155)	0.226 ± 0.00598 (161)
LMM	Baseline I - 11 Hz	Baseline II - 30 Hz
Average rate	β=1.53, p=0.134	β=1.06, p=0.395
Max rate	β=0.896, p=0.691	β=2.51, p=0.427
Interspike interval cv	β=-0.3, p=0.0284	β=-0.17, p=0.144
Burst event ratio	β=0.00905, p=0.444	β=-0.0228, p=0.00607
Speed score	β=-0.00589, p=0.64	β=0.0347, p=0.00256
Head mean vec len	β=-0.0163, p=0.721	β=-0.00405, p=0.798
Border score	β=-0.0106, p=0.276	β=-0.00189, p=0.882
LMM	Baseline I - Baseline II	11 Hz - 30 Hz
Average rate	β=1.4, p=0.589	β=0.537, p=0.561
Max rate	β=2.86, p=0.068	β=3.02, p=0.269
Interspike interval cv	β=-0.0853, p=0.398	β=0.0142, p=0.903
Burst event ratio	β=0.0034, p=0.71	β=-0.0248, p=0.0107
Speed score	β=-0.0184, p=0.215	β=0.0243, p=0.139
Head mean vec len	β=-0.0136, p=0.0349	β=0.00276, p=0.807
Border score	β=-0.0025, p=0.832	β=0.00672, p=0.654

Table S6: **Statistics for BS not grid cell firing properties** Shows weighted mean ± standard error of the mean and number of units (n) and results from a linear mixed model, β and p denotes effect size and p value respectively.

Supplementary discussion related to Figure 3

Our results differ from (*13*) on the number of detected phase precessing and recessing units recorded from MEC during baseline conditions.

The main difference in analysis from the results presented in this study and that of Reifenstein et al. (*13*) is in-field separation and the fact that we used a python based scientific library (minimizer etc.). This is unlikely to cause such a difference in results, and indeed, by reanalyzing publicly available data from Sargolini et al. (*37*) we were able to reproduce results from Reifenstein et al. (*13*). Looking at this data we performed an additional control comparing detection of phase precession with a "random" band (20-25 Hz). It is both interesting and alarming that assessment of single run phase precession showed such a high degree of false positives (Fig. S7), but it might be expected due to small sample size (*80*). Single run phase precession is probably a real phenomenon, but using the analysis outlined in (*36, 56, 13*) to assess it might be unfortunate as there might be many field crossings that simply do not phase precess, even if the circular linear regression is obtained from a good fit of the model, due to the low number of spikes found from a single crossing. Moreover, when comparing our reanalysis of the Sargolini (*37*) data to results from Reifenstein et al. (*13*) we were not able to reproduce a distribution of slopes from single pass data using the same slope limit as in Reifenstein et al. In our data we have therefore used a different slope limit. This posed a challenge to our analysis, but when assessing the distribution of R we found that using the slope limits from Reifenstein ([-100,100] rad/m) this indicated overfitting as seen by a shift towards $R = 1$ in Fig. S7d compared with c using [-20,20] rad/m. When adding additional criteria from goodness of fit ($R > 0.1$) during Baseline II we found a change in the distribution of precession/recession, which might indicate that phase relations can vary with time. This may indicate that spikes relation to phase can be modulated by MSA inputs, possibly providing control of how a neuron's activity relates to the phase of theta. Moreover, this might indicate that spikes from grid cells are more robustly related to space than theta phase. Thus, using phase relations as a code for spatial position might be problematic. If, for example, there is some context dependence to how a neuron's activity relates to the phase of theta, the information of position might be difficult to decode from phase alone. At the extreme of scepticism, phase precession and recession in MEC might just be an epiphenomenon.